Phase Diagram and Electrical Conductivity of CeBr$_3$-KBr

Leszek Rycerz[a], Ewa Ingier-Stocka[a], Slobodan Gadzuric[b, c], and Marcelle Gaune-Escard[b]

[a] Chemical Metallurgy Group, Faculty of Chemistry, Wroclaw University of Technology,
Wybrzeze Wyspianskiego 27, 50-370 Wroclaw, Poland
[b] Ecole Polytechnique, Mecanique Energetique, Technopôle de Chateau-Gombert,
5 rue Enrico Fermi, 13453 Marseille Cedex 13, France
[c] Faculty of Natural Science, Department of Chemistry, University of Novi Sad,
Trg. Obradovica 3, 21000 Novi Sad, Serbia

Reprint requests to Prof. M. G.-E.; Fax: +33 4 91 11 74 39; E-mail: mge@polytech.univ-mrs.fr

This paper continues our research program on lanthanide halide-alkali metal halide systems. Differential scanning calorimetry (DSC) was used to investigate the phase equilibria of the CeBr$_3$-KBr system. This system is characterized by the two congruently melting compounds K$_3$CeBr$_6$ and K$_2$CeBr$_5$ and the three eutectics located at the CeBr$_3$ mole fractions 0.193 (837 K), 0.295 (855 K) and 0.555 (766 K). K$_3$CeBr$_6$ forms at 775 K and melts congruently at 879 K with the related enthalpies 54.5 and 41.7 kJ mol^{-1}, respectively. K$_2$CeBr$_5$ melts congruently at 874 K with the enthalpy 82.4 kJ mol^{-1}. The electrical conductivity was measured of all CeBr$_3$-KBr mixtures and of the pure components down to temperatures below solidification. The experimental determinations were conducted over the entire composition range in steps of about 10 mol%. The specific electrical conductivity decrease with increasing CeBr$_3$ concentration, with significantly larger conductivity changes in the potassium bromide-rich region. The results are discussed in terms of possible complex formation.

Key words: Cerium Bromide; Potassium Bromide; Phase Diagram; Electrical Conductivity;
Differential Scanning Calorimetry.

1. Introduction

The present work continues our research program on lanthanide halide-alkali metal halide systems. We focused our studies on these systems for two reasons: Firstly, rare-earth metals play a significant role in sophisticated industrial applications. Secondly, data on lanthanide compounds are scarce and not easily accessible.

Data on LaBr$_3$-MBr (M = K, Rb, Cs) were obtained from thermal, electrochemical and structural measurements by Seifert and Yuan [1], while phase diagrams of other LaBr$_3$-MBr systems were obtained from thermal measurements only [2, 3]. Data on the thermodynamic properties of CeBr$_3$-MBr systems are missing. Thermodynamic and electrical conductivity results on the tribromide systems NdBr$_3$-LiBr [4], TbBr$_3$-NaBr [5], LaBr$_3$-LiBr [6] and CeBr$_3$-LiBr [7] were already obtained by us. The present work is devoted to phase equilibria and the electrical conductivity of CeBr$_3$-KBr.

2. Experimental

2.1. Chemicals

Cerium(III) bromide was synthesized from cerium(III) carbonate hydrate (Aldrich, 99.9%). Ce$_2$(CO$_3$)$_3 \cdot x$H$_2$O was dissolved in hot concentrated HBr. The solution was evaporated and CeBr$_3 \cdot x$H$_2$O was crystallized. Ammonium bromide was then added, and this wet mixture of hydrated CeBr$_3$ and NH$_4$Br was first slowly heated to 450 and then to 570 K to remove the water. The resulting mixture was subsequently heated to 650 K for sublimation of NH$_4$Br. Finally the salt was melted at 1100 K. Crude CeBr$_3$ was purified by distillation under reduced pressure ($\sim$ 0.1 Pa) in a quartz ampoule at 1150 K. CeBr$_3$ prepared in this way had a purity of min. 99.9%.

Potassium bromide was a Merck Suprapur reagent (minimum 99.9%). Before use, it was progressively heated to fusion under gaseous HBr. Excess of HBr was then removed from the melt by argon bubbling.
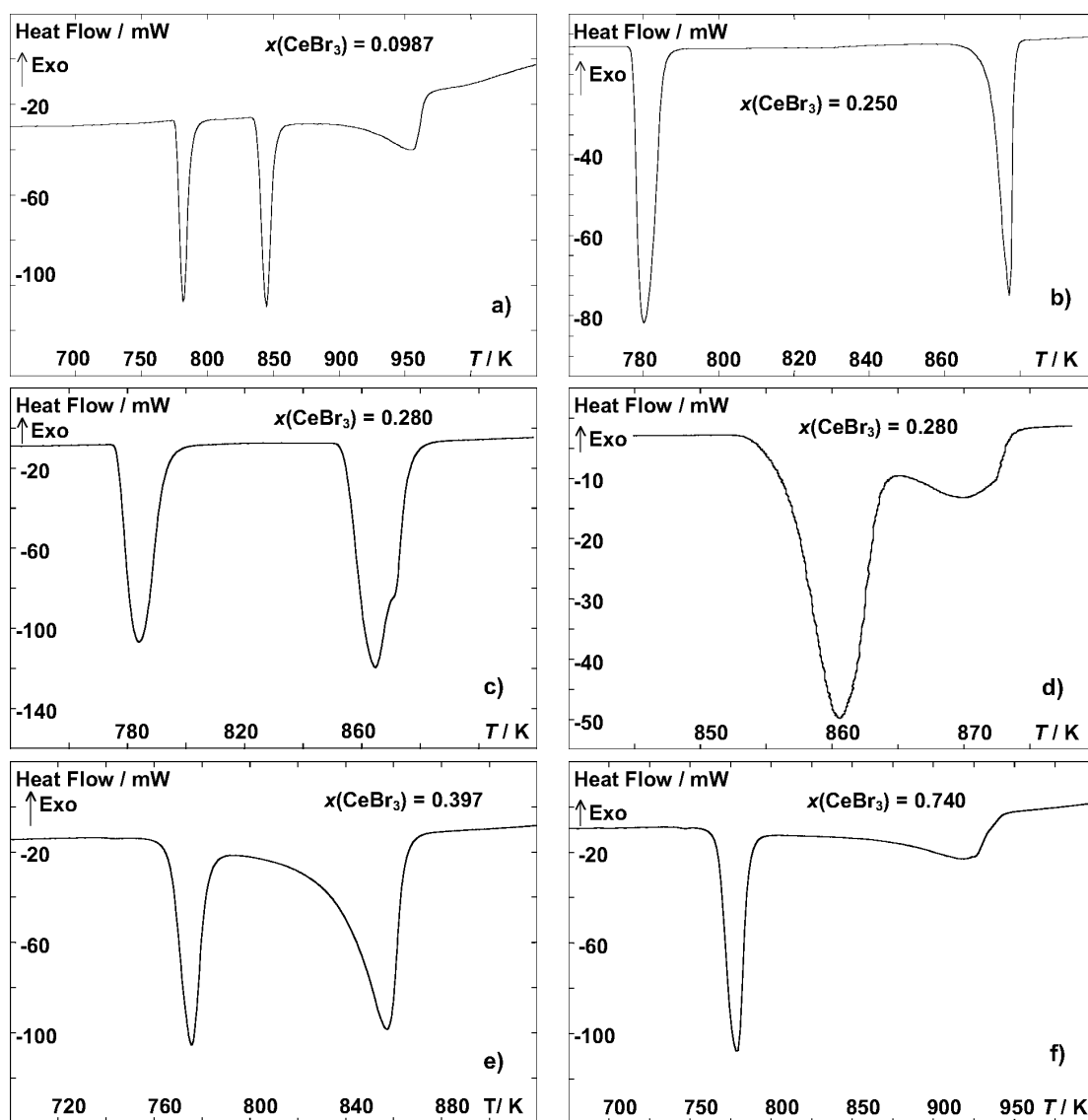
Fig. 1. DSC heating curves for selected xCeBr$_3$ - $(1-x)$KBr mixtures: (a) $x = 0.0987$, heating rate = 5 K min^{-1}; (b) $x = 0.250$, heating rate = 5 K min^{-1}; (c) $x = 0.280$, heating rate = 5 K min^{-1}; (d) $x = 0.280$, heating rate = 0.2 K min^{-1}; (e) $x = 0.397$, heating rate = 5 K min^{-1}; (f) $x = 0.740$, heating rate = 5 K min^{-1}.

The appropriate amounts of CeBr$_3$ and KBr were melted in vacuum-sealed quartz ampoules. The melts were homogenized and solidified. These samples were ground in an agate mortar in a glove box. Homogenous mixtures of different compositions were prepared in this way and used for phase diagram and electrical conductivity measurements.

All chemicals were handled inside a high purity argon atmosphere in a glove box (water content < 2 ppm).

2.2. Measurements

The temperatures and enthalpies of the phase transitions of CeBr$_3$-KBr mixtures were measured with a Setaram DSC 121 differential scanning calorimeter. This Calvet-type apparatus, which can be operated between 150 and 1100 K, and the measurement procedure were described in detail in [8, 9]. Calibration of the apparatus was performed by the "Joule effect" [9] and checked by measurements of temperatures and en-
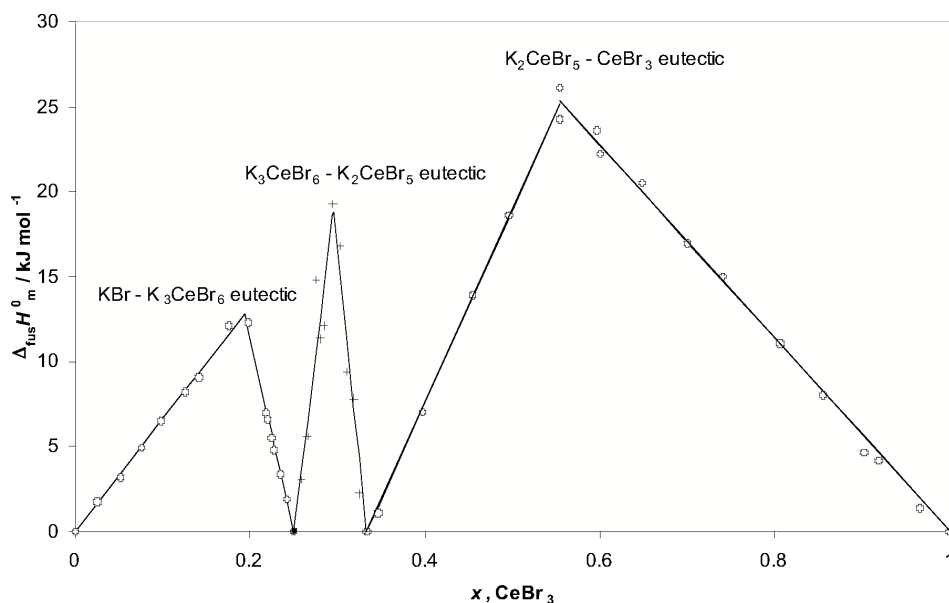
Fig. 2. Tamman diagram of the CeBr₃-KBr system.

thalpies of phase transitions of standard substances. Results obtained (differences in fusion temperatures less than 1 K, differences in enthalpies of fusion less than 0.5%) confirmed the correct work of the calorimeter.

Samples of $300-500$ mg were contained in quartz ampoules (about 6 mm diameter, 15 cm length) and sealed under reduced pressure of argon. The sidewalls of the ampoules were ground in order to fit the cells snugly into the heat flow detector. Experiments were conducted at heating and cooling rates ranging between 5 and 0.2 K min^{-1}. Only the heating curves were analyzed to gather data of temperatures and enthalpies, because supercooling was observed during cooling. Temperatures of transitions and eutectic effects were taken as T_{onset} of corresponding differential scanning calorimetry (DSC) peaks, whereas liquidus temperatures were taken as T_{peak} (temperature of peak maximum). The temperatures were determined with experimental errors less than ± 1 K.

Electrical conductivity measurements were carried out in a capillary quartz cell with cylindrical platinum electrodes as described in [10]. The conductivity of the melt was measured with the conductivity meter Tacussel CDM 230. Experimental runs conducted both upon heating and cooling regimes at a rate of 1 K min^{-1} showed a reproducibility within 1% of these two series; an average value was used in further calculations. The accuracy of the electrical conductivity measurements was estimated to be $\pm 2\%$. The temperature was

measured by means of a Pt/Pt-Rh thermocouple within 1 K. Experimental cells were calibrated in the same temperature range with pure KCl melt, as described in [11]. All measurements were carried out under argon atmosphere.

3. Results

3.1. Phase Diagram

The CeBr₃-KBr phase diagram was determined after DSC measurements performed on samples with 46 different compositions. Some characteristic thermograms are presented in the Figure 1. In all heating runs, the peak at the highest temperature corresponds to the liquidus temperature.

In the composition range $0 < x < 0.250$, three endothermic peaks were present in all heating thermograms (Fig. 1a, $x = 0.0987$). The first one, at 776 K, is observable in all thermograms up to $x = 0.333$, where it disappears. The second one, observed in all samples up to $x = 0.250$ at 837 K, can be undoubtedly ascribed to the KBr-K₃CeBr₆ eutectic. As quoted previously, the third peak corresponds to the melting temperature. The KBr-K₃CeBr₆ eutectic contribution to the enthalpy of fusion was determined and is plotted against the composition in Figure 2. This so-called Tamman construction makes it possible to evaluate the eutectic composition accurately from the intercept of the two linear parts in Fig. 2, as $x = (0.193 \pm 0.002)$.
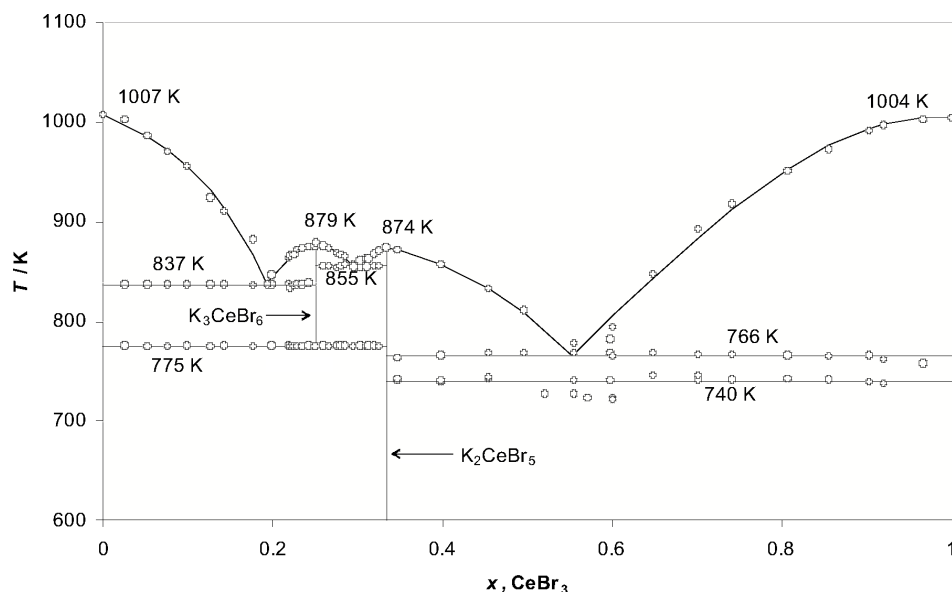
Fig. 3. Phase diagram of the CeBr$_3$-KBr system.

The eutectic mixture melts with the enthalpy $\Delta_{fus}H_m = (12.8 \pm 0.3)$ kJ mol^{-1}. In this Tamman construction it was assumed that there was no solubility in the solid state. Thus the straight lines intercept the composition axis at $x = 0$ and $x = 0.250$.

For the mixture with $x = 0.250$ only peaks at 776 and 879 K were observed on the thermograms (see Fig. 1b). The latter peak has the typical shape of a congruently melting compound. We deduced that a congruently melting K$_3$CeBr$_6$ compound exists in the CeBr$_3$-KBr system. Taking into account the high value of the enthalpy related to the peak at 776 K [(54.5 ± 0.5) kJ mol^{-1}], which is characteristic for M$_3$LnX$_6$ compound formation from MX and M$_2$LnX$_5$ [12, 13], one can conclude that also the peak at 776 K is related to K$_3$CeBr$_6$ formation from KBr and K$_2$CeBr$_5$. This compound melts congruently at 879 K with a related enthalpy of (41.7 ± 0.3) kJ mol^{-1}.

In the composition range $0.250 < x < 0.333$, on the curves registered with a heating rate of 5 K min^{-1} only two endothermic peaks were visible at 776 and 855 K (see Fig. 1c), independently on the composition. The effect at 776 K, related to K$_3$CeBr$_6$ formation, disappeared at $x = 0.333$. It suggests that at this composition another compound, namely K$_2$CeBr$_5$, exists in the CeBr$_3$-KBr system. This finding agrees with the previously quoted K$_3$CeBr$_6$ formation from KBr and K$_2$CeBr$_5$. The strange result concerning the effect at higher temperature (855 K), led us to the conclusion that this peak must be the result of overlapping of

several peaks. DSC measurements were conducted on samples with x varying from 0.250 to 0.333 with a low heating rate (0.2 K min^{-1}) – in order to separate thermal effects. Indeed one peak, visible on thermograms performed with a heating rate of 5 K min^{-1} at about 855 K, was separated into two (Fig. 1d): The first one at 855 K can undoubtedly be attributed to the K$_3$CeBr$_6$-K$_2$CeBr$_5$ eutectic (it disappeared for $x = 0.250$ and 0.333) and the second at different temperatures corresponds to the liquidus. The K$_3$CeBr$_6$-K$_2$CeBr$_5$ eutectic contribution to the enthalpy of fusion was determined and is plotted against the composition in Fig. 2 in order to determine accurately the eutectic composition. The intercept of the two linear parts in Fig. 2 gives this composition as $x = (0.295 \pm 0.005)$. The mixture with the eutectic composition melted with an enthalpy $\Delta_{fus}H_m$ of about (18.8 ± 2.0) kJ mol^{-1}. In this Tamman construction it was assumed that there was no solubility in the solid state, thus the straight lines intercept the composition axis at $x = 0.250$ and $x = 0.333$.

K$_2$CeBr$_5$ was found to melt congruently at 874 K with the related enthalpy (82.4 ± 0.5) kJ mol^{-1}.

In the composition range $0.333 < x < 1.00$ two well shaped peaks are present on the DSC curves (Figs. 1e, f). The first, observed at 766 K, corresponds to the K$_2$CeBr$_5$-CeBr$_3$ eutectic, the next to the liquidus temperature. The K$_2$CeBr$_5$-CeBr$_3$ eutectic contribution to the enthalpy of fusion, determined and plotted against the composition in Fig. 2, gives the eutectic composition $x = (0.555 \pm 0.007)$. The mixture with the
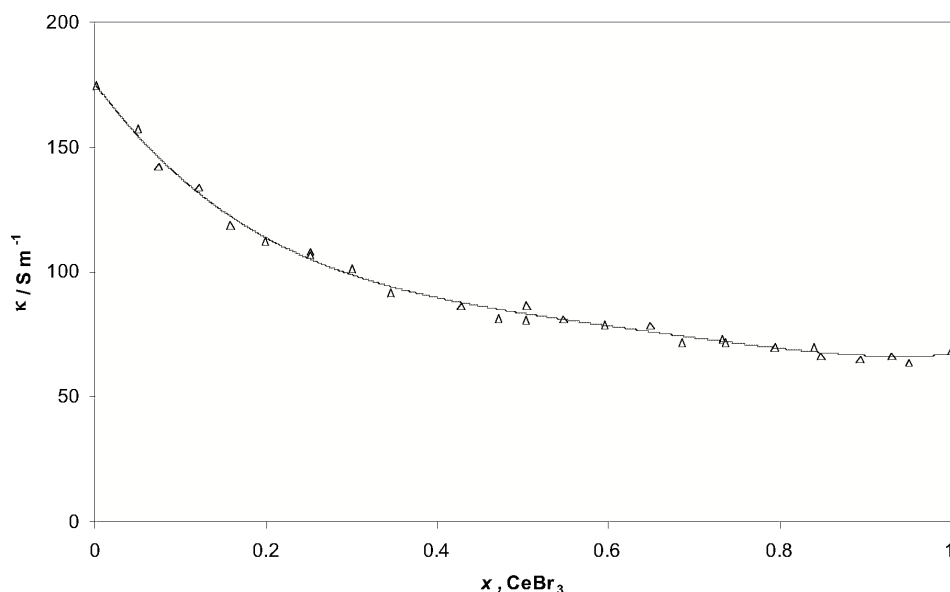
Fig. 4. Electrical conductivity isotherm of CeBr₃-KBr liquid mixtures at 1050 K.

eutectic composition melts with an enthalpy $\Delta_{fus}H_m$ of about (25.3 ± 0.6) kJ mol^{-1}. In the calculation it was assumed that there was no solubility in the solid state, thus the straight lines intercept the composition axis at $x = 0.333$ and $x = 1$. The origin of the additional and very weak thermal effect (less than 0.1 kJ mol^{-1} independently from the composition of the mixtures with $0.333 < x < 1.00$), observed in the DSC thermograms at ~ 740 K cannot be explained yet. Additional information is expected from structural studies, which are planned in the near future.

The phase diagram, constructed on the basis of the above measurements, is presented in Figure 3.

3.2. Electrical Conductivity

The electrical conductivity was measured for the pure components and for several liquid CeBr₃-KBr mixtures. The experimental determinations were conducted over the entire composition range in steps of about 10 mol%. In Fig. 4 the experimental conductivity isotherm at 1050 K, covering the whole composition range, is plotted against the mole fraction of CeBr₃. The specific conductance decreased with increasing CeBr₃ content, with significantly larger conductivity changes in the potassium bromide-rich region. We observed this general tendency in earlier studied lanthanide halide-alkali metal halide binary systems [6, 14–20].

The classical Arrhenius equation

$$\kappa = \kappa_o \exp(-E_A/RT) \qquad (1)$$

was tested for all studied mixtures. For the majority of our experimental data the plot of the dependence $\ln \kappa = f(1/T)$ deviates from linearity (see Fig. 5). So, the activation energy was evaluated by the equation

$$E_A(T) = -R[A_1 + 2A_2(1/T)], \qquad (2)$$

where R is the gas constant and A_1, A_2 are coefficients determined by the least-squares method from the equation

$$\ln \kappa = A_0 + A_1 \cdot 10^3 \cdot (1/T) + A_2 \cdot 10^6 \cdot (1/T)^2. \qquad (3)$$

All A_i coefficients are listed in Table 1, together with the E_A values determined at 1050 K for all CeBr₃-KBr mixtures. As indicated above, the activation energy of the conductivity changes with the temperature in every individual mixture, validating the early statement made by Yaffe and van Artsdalen [21, 22] of a correlation with structural changes in melts.

Raman spectroscopic investigations [23] showed that octahedral LnBr₆³⁻ ions are formed in LnBr₃-MBr liquid mixtures. These ions constitute the predominant species in MBr-rich liquid mixtures. As the LnBr₃ content increases, distorted octahedral species occur, which are bridged by bromide anions. Complex formation in the melt influences the activation energy

x (CeBr$_3$)	Temp. range (K)	A_0 (S m^{-1})	A_1 (S m^{-1} K)	A_2 (S m^{-1} K^2)	ln(s)	n	E_A at 1050 K (kJ mol^{-1})
0.000	1020–1122	5.9635	−0.3176	−0.5468	0.0008	263	11.300
0.049	1022–1165	5.0271	1.5227	−1.5606	0.0017	350	12.055
0.073	962–1146	4.7900	1.9039	−1.8112	0.0150	851	12.853
0.120	953–1155	6.6851	−2.1862	0.3090	0.0134	477	13.282
0.157	878–1164	5.3585	0.4932	−1.1584	0.0147	648	14.245
0.198	851–1155	5.4117	0.2119	−0.9793	0.0033	1329	13.747
0.251	881–1175	5.1557	0.7328	−1.2992	0.0053	650	14.482
0.300	877–1131	5.3340	0.2218	−1.0171	0.0003	875	14.263
0.345	872–1169	5.1341	0.5023	−1.2010	0.0012	745	14.844
0.426	841–1142	4.5394	1.7109	−1.8836	0.0042	1388	15.604
0.502	868–1165	4.4139	2.0654	−2.1886	0.0015	638	17.488
0.546	796–1138	3.3092	4.4371	−3.4522	0.0053	764	17.780
0.590	809–1155	4.3032	2.2475	−2.2517	0.0101	1455	16.973
0.648	869–1164	4.0165	3.3051	−3.0825	0.0020	666	21.336
0.732	929–1143	4.0512	3.3095	−3.2071	0.0016	487	23.274
0.794	943–1145	4.1880	3.0472	−3.1295	0.0015	961	24.225
0.839	1014–1163	5.1850	1.1143	−2.200	0.0026	367	25.575
0.893	994–1162	4.8165	1.8065	−2.5983	0.0011	438	26.129
0.930	1036–1164	5.3724	0.7680	−2.002	0.0034	305	26.873
0.951	1010–1164	4.4519	2.7234	−3.1839	0.0035	360	27.778
1.000	988–1123	0.0014	12.2264	−8.1698	0.0095	1345	27.729

Table 1. Coefficients of the equation: $\ln \kappa = A_0 + A_1 (1000/T) + A_2 (1000/T)^2$ and the activation energy of the electrical conductivity (E_A) of liquid CeBr$_3$-KBr mixtures at 1050 K. κ in S m^{-1}; ln(s), standard deviation of ln κ; n, number of experimental data points.
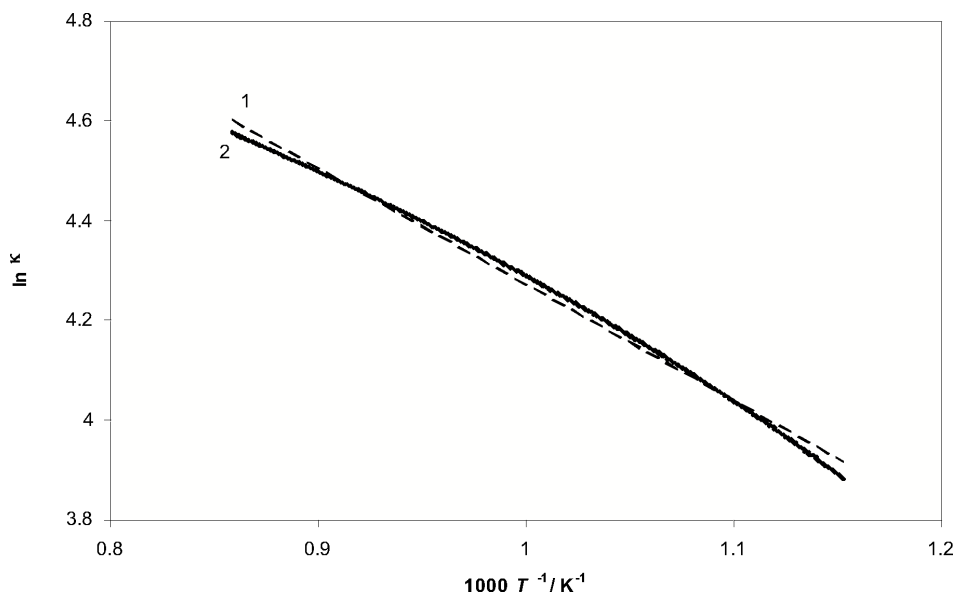

Fig. 5. ln κ vs. 1000/T of molten CeBr$_3$-KBr mixture, x(CeBr$_3$) = 0.502; 1, Arrhenius equation (1); 2, equation (3) of this work.

for the electrical conductivity, which should increase with increasing amount of complexes formed. This was observed indeed in the CeBr$_3$-MBr systems. However, some differences were found between CeBr$_3$-LiBr [7, 24] and CeBr$_3$-NaBr [24] on one hand, and the CeBr$_3$-KBr system on the other. Figure 6 shows the activation energy at 1050 K as function of the composition for CeBr$_3$-MBr systems (M = Li, Na, K). Whereas in the systems with LiBr and NaBr the activation energy increases smoothly with the CeBr$_3$ content, in the

system with KBr it increases up to about 10 mol% of CeBr$_3$, and becomes almost stable up to 40 mol% of CeBr$_3$. This plateau can be explained in terms of the coexistence of different forms of complexes, as evidenced by Raman spectroscopy [23]. The observed concentration evolution of E_A values is similar to that observed in LaBr$_3$-MBr (M = K, Rb, Cs) binary systems [15].

The activation energy of electrical conductivity increases with the alkali metal cationic radius (from
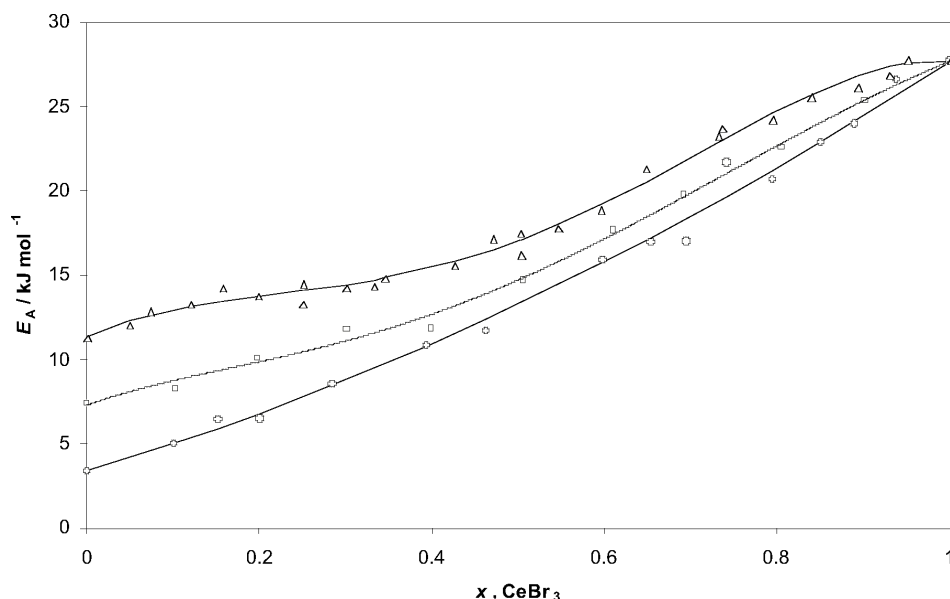
Fig. 6. Activation energy at 1050 K of CeBr₃-MBr liquid mixtures. Open circles, M = Li; open squares, M = Na; open triangles, M = K.

lithium to potassium). It is likely that this is due to a complex concentration increase in the melt. This observation agrees with the mixing enthalpy measurements [25], that also showed that the formation enthalpy, attributed to the $CeBr_6^{3-}$ complex ions formation, increases with the ionic radius of the alkali metal cation. Thus, the presence of KBr in mixtures with CeBr₃ favours the expected complex ion formation more than addition of NaBr and results in a larger enthalpy of formation, larger activation energy for conductivity, etc.

Acknowledgements

[1] H. J. Seifert and Y. Yuan, J. Less-Common Metals **170**, 135 (1991).

[2] G. Vogel, Z. anorg. allg. Chem. **388**, 43 (1972).

[3] R. Blachnik and A. Jaeger-Kasper, Z. anorg. allg. Chem. **46**, 74 (1980).

[4] L. Rycerz, E. Ingier-Stocka, M. Cieslak-Golonka, and M. Gaune-Escard, J. Thermal. Anal. Cal. **72**, 241 (2003).

[5] L. Rycerz, M. Cieslak-Golonka, E. Ingier-Stocka, and M. Gaune-Escard, J. Thermal Anal. Cal. **72**, 231 (2003).

[6] L. Rycerz, E. Ingier-Stocka, B. Ziolek, S. Gadzuric, and M. Gaune-Escard, Proceedings of the International Symposium on Ionic Liquids in Honour of Professor Marcelle Gaune-Escard (Eds. H. A. Øye and A. Jagtøyen), Carry le Rouet, France, June 26 – 28, 2003, p. 83.

[7] E. Ingier-Stocka, L. Rycerz, S. Gadzuric, and M. Gaune-Escard, Proceedings of the 7th International Symposium on Molten Salts Chemistry and Technology, MS 7, August 29 – September 2, 2005, Toulouse, France, p. 829.

[8] M. Gaune-Escard, L. Rycerz, W. Szczepaniak, and A. Bogacz, J. Alloys Comp. **204**, 193 (1994).

[9] L. Rycerz, High Temperature Characterization of LnX₃ and LnX₃-AX Solid and Liquid Systems (Ln = Lanthanide, A = Alkali, X = Halide): Thermodynamics and Electrical Conductivity, Ph. D. Thesis, Université de Provence Aix-Marseille I, France 2003.

[10] Y. Fouque, M. Gaune-Escard, W. Szczepaniak, and A. Bogacz, J. Chim. Phys. **75**, 360 (1978).

[11] G. J. Janz, Mater. Sci. Forum **73 – 75**, 707 (1991).

[12] L. Rycerz and M. Gaune-Escard, Inorg. Chem. **46**, 2299 (2007).

[13] L. Rycerz, Scientific Papers of the Institute of Inorganic Chemistry and Pure Elements of the Wroclaw University of Technology, No. 68, 2004 (in Polish).

[14] L. Rycerz, E. Ingier-Stocka, M. Cieslak-Golonka, and M. Gaune-Escard, J. Thermal. Anal. Cal. **72**, 241 (2003).

[15] B. Ziolek, L. Rycerz, S. Gadzuric, E. Ingier-Stocka, and M. Gaune-Escard, Z. Naturforsch. **60a**, 75 (2005).

[16] S. Gadzuric, E. Ingier-Stocka, L. Rycerz, and M. Gaune-Escard, Z. Naturforsch. **59a**, 77 (2004).

[17] E. Ingier-Stocka, S. Gadzuric, L. Rycerz, M. Cieslak-Golonka, and M. Gaune-Escard, J. Nucl. Mater. **344**, 120 (2005).

[18] E. Ingier-Stocka, S. Gadzuric, L. Rycerz, and M. Gaune-Escard, J. Alloys Comp. **397**, 63 (2005).

[19] E. Ingier-Stocka, L. Rycerz, S. Gadzuric, and M. Gaune-Escard, Proceedings of the 7th International Symposium on Molten Salts Chemistry and Technology, MS 7, August 29 – September 2, 2005, Toulouse, France, pp. 829 – 831.

[20] E. Ingier-Stocka, S. Gadzuric, L. Rycerz, and M. Gaune-Escard, Proceedings of the Euchem 2004 Molten Salts Conference, Piechowice, Poland, June 20 – 25, 2004, p. 170.

[21] E. R. van Artsdalen and J. S. Yaffe, J. Phys. Chem. **59**, 118 (1955).

[22] J. S. Yaffe and E. R. van Artsdalen, J. Phys. Chem. **60**, 1125 (1956).

[23] G. M. Photiadis, B. Borresen, and G. N. Papatheodorou, J. Chem. Soc. Faraday Trans. **17**, 2605 (1998).

[24] E. Ingier-Stocka, L. Rycerz, S. Gadzuric, and M. Gaune-Escard, J. Alloys Comp. (in press).

[25] L. Rycerz and M. Gaune-Escard, unpublished results.